Mar Geophys Res (2007) 28:13–26
DOI 10.1007/s11001-006-9011-4

ORIGINAL PAPER

The Bremen ocean bottom tiltmeter (OBT) – a technical article on a new instrument to monitor deep sea floor deformation and seismicity level

Marcus Fabian · Heinrich Villinger

Received: 22 December 2005 / Accepted: 16 October 2006 / Published online: 14 February 2007

Abstract The Bremen ocean bottom tiltmeter is a new 6000 m-depth deep sea instrument for autonomous observation of sea floor tilt with signal periods longer than 7.5 s. The instrument also records vertical acceleration in the frequency range from DC to 1 Hz. The tiltmeter has an Applied Geomechanics Inc. 756 wide angle biaxial bubble tilt sensor with a resolution of 1.0μ rad (0.2 arc second). A Kistler Corp. MEMS accelerometer of type Servo K-Beam 8330A2.5 with about 10^{-5}m/s^2 resolution is used for the acceleration measurements. An Oceanographic Embedded Systems AD24 24 bit Sigma-Delta converter, which is controlled by a low-power Persistor Inc. embedded computer system of type CF 2, samples the data. The duration of tiltmeter operation is more than one year, which is controlled by the battery life. In our design the tiltmeter does not need active leveling devices, i.e., servo motors or other moving components to adjust sensors or frame. We designed the instrument for deployments by means of a remote operated vehicle. Since May 2005 the Bremen ocean bottom tiltmeter has recorded sea floor deformation and seismicity level in the Logatchev hydrothermal vent field, Mid-Atlantic Ridge. The tiltmeter is a part of the monitoring system of project 'Logatchev Long-Term Environmental Monitoring,' called LOLEM, of the German research program with the name 'Schwerpunktprogramm 1144: Vom Mantel zum Ozean.'

M. Fabian (✉) · H. Villinger
Department 5 Geosciences, Sea Technics/Sensors, University of Bremen, Klagenfurter Straße, Bremen D-28359, Germany
e-mail: marcus.fabian@uni-bremen.de

Keywords Logatchev hydrothermal vent field · Long-term monitoring · Low power data logging · MEMS accelerometer · Mid Atlantic Ridge · Ocean bottom tiltmeter · Offshore precision measurements

Introduction

Hydrothermal activity at mid-ocean ridges, like diffuse venting and black or white smoker outflow, is controlled in space and time by a number of geodynamic processes (Cooper and Elderfield 2000; Fornari et al. 1998; Goto et al. 2002; Kingston-Tivey et al. 2002). Davis and Becker (1999), Eberhart et al. (1988) and Crone and Wilcock (2005) have investigated the influence of ridge tectonic activity on hydrothermalism. Kasahara and Sato (2001), for instance, explored the tidal loading influence on hydrothermal systems. German and Parson (1998) and Wright et al. (1995) worked on the geological structure and the influence of deeper magmatic processes on the Mid-Atlantic Ridge. In contrast, sea floor deformation and magma chamber inflation or deflation, as well as earthquake activity on the Juan de Fuca Ridge were assessed by Tolstoy et al. (1998, 2002), Chadwell et al. (1999) and Chadwick et al. (1999, 2006).

Despite several studies on these hydrothermal processes, investigations have mostly depended on short observation periods or single samples. Continuous long-term development of hydrothermal systems is very sparsely observed. On the other hand, it is assumed that during long time spans, hydrothermal systems contribute a significant amount to the bulk chemistry of the oceans and magmatic events can affect the vent chemistry (Lilley et al. 2003). Hydrothermal systems harbour a rich array of biological communities, but, because of the scarcity of long-term data, predictions of budget- or process-models are not very reliable (Tyler and Young 2003). There is thus an urgent need for instruments and experimental set-ups that can provide the necessary environmental data over long time periods and with high precision. Two key environmental variables, which are directly related to ground dynamic processes, are sea floor tilt and acceleration.

Results from local and regional tilt measurements on land and on the sea floor (Anderson et al. 1997; Tofani and Horath 1990) demonstrate that these parameters are valuable indicators of ground deformation, which are generated over various time scales. For instance, such ground deformations may be triggered by changes in subsurface fluid flow (Fabian and Kümpel 2003; Fabian 2004; Jahr et al. 2005; Vasco et al. 2002), tidal loading (Sleeman et al. 2000; Tolstoy et al. 1998; Tolstoy et al. 2002) or tectonic activity (Bilham and Beavan 1979; Savage et al. 1979).

Tilt monitoring provides quasi-continuous high precision data of seafloor dynamics at any given site. Therefore, these data provide information about processes, which might take place between those times at which single, non-continuous measurements are done on the same site by other methods, or at which only singular samples have been collected. Hence, quasi-continuous tilt data are useful to fill the general gap of information between regular monitoring opportunities e.g., fluid sampling or collecting biological species during a research cruise. On-shore, continuous tilt measurements are used to interpolate data collected during geodetic campaigns of GPS, leveling and gravimetry on reference-points, e.g. (Campbell et al. 2002; Kümpel et al. 2001; Kümpel and Fabian 2003). Offshore, a comparable combination of tilt measurements coupled with acoustic techniques described by Spiess et al. (1998) and Gagnon et al. (2005), or with the sea floor leveling techniques described by Chadwick et al. (2006) is also possible.

The Bremen ocean bottom tiltmeter (OBT) is designed as a monitoring tool for processes, which are related to slow ground deformation, i.e., deformation with signal periods from minutes to months, e.g., caused by magmatic activity, crustal formation and fluid circulation in the upper sea floor.

As a complementary parameter to tilt, the OBT also records vertical acceleration in the low frequency range from DC to 1 Hz. To sense these signals, a Micro-Electro-Mechanical System (MEMS) accelerometer (Bernstein et al. 1999; Moore and Syms 1999; Varadan and Varadan 2000) is implemented in the OBT. Geophysical studies using these MEMS sensors, especially in the low frequency range below 1 Hz, are quite rare. Nonetheless, technical sensor data, our own laboratory tests, the report of the vendor (Kistler 2004) and commercial applications (Holland 2003) demonstrate that these sensors have enough sensitivity to register even weak ground accelerations. The sensor we use, has a nominal resolution of about 10^{-5}m/s^2, which is close to the background noise level on the sea floor. Crawford and Webb (2000) show that ocean floor noise spectra has a comparable level. Therefore, the sensor is best suited to detect accelerations, which are not covered by sea floor background noise.

For our measurements with the OBT in the Logatchev hydrothermal vent field (Mazarovich and Sokolov 1998), we expect ground acceleration related to tremor-like seismicity, which might be caused by hydrothermally forced fluid flow and circulation in the upper subsurface or which is generated by tectonic activity. Mcclain et al. (1993) and Sohn et al. (1995) report on these types of signals from the northern and the southern Juan de Fuca Ridge, respectively. Fox (1999) and Tolstoy et al. (2002) show similar data, measured on Axial Volcano, Juan de Fuca Ridge. Chouet (1996) reported on long-period volcano seismicity on-shore. These studies present seismic signals, which have a highly variable wave form pattern that differs between single seismic events. The seismic events originate from different sources in the upper subsurface where wave-trains overlay each other. Accordingly, the signal amplitude is highly variable from signal to signal and can hardly be estimated. The strongest signal components are reported to be in the frequency range between 1 and about 50 Hz, which is above the measuring range of the OBT. Therefore, acceleration data from the OBT (or low-frequency seismicity level) are regarded as a proxy for background hydrothermal and tectonic activity in the Logatchev hydrothermal vent field. An intensified activity level, which might be related to local tremors or regional earthquakes, can indicate possible changes in stress field and alterations in the subsurface fracture system that serves as pathways for hydrothermal fluids (Fisher et al. 1996).

Here we provide an overview of our design concept of the OBT and present in detail the selected sensors and data logger. We also report on relevant technical details and show laboratory data for validation. We point out differences with other designs known from ocean bottom seismometers (OBS), ocean bottom hydrophones (OBH) and other OBT. Finally, we summarize the deployment of our OBT in the Logatchev hydrothermal vent field at the Mid-Atlantic Ridge (Lackschewitz et al. 2005), which was done in May

2005 by means of the remote operated vehicle (ROV) of 'Zentrum für Marine Umweltwissenschaften' (MARUM) of the University of Bremen.

Design concept

Development of the OBT requires a problem specific selection and design of sensor components, pressure cases and a supporting sensor frame. One has to take into account (1) adequate sensor resolution, (2) low power consumption and suitability of data logger for autonomous operation, (3) good coupling to the ground, (4) uncomplicated leveling and remote-controlled installation on the sea floor and (5) robustness against high pressure, sea water and handling by a ROV and on board a research vessel.

Generally, our main strategy was to maximize reliability and to minimize the number of error sources by using approved off-the-shelf components and by using as few components as possible. As we can use a ROV for deployment and recovery we do not need a release and pop-up mechanism with buoyancy, as often used in OBS and OBH surveys, e.g. (Bialas and Flueh 1999; Kovachev et al. 1997; Suetsugu et al. 2005). This allows a compact and rigid construction that has a minor drag in bottom currents. Furthermore, in contrast with the designs of Shimamura and Kananzawa (1988) and Tolstoy et al. (1998, 2002) we omit adjusting devices or other mechanical or electronic components to level the frame of the OBT or its sensors.

The model of the OBT shown in Fig. 1 gives an overview of the instrument and its consistuent parts. The aluminium frame consists of a triangular base plate, a bar for handling and three legs with hollow tips. An aluminium pressure case, which is screwed to

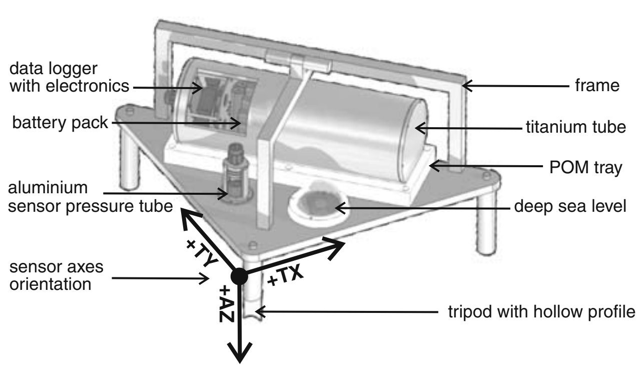

Fig. 1 CAD-model of the OBT. Physical dimensions of the base plate: 0.85 m (long edge) × [0.6 × 0.6 m]. Height of the OBT: 0.45 m, weight in water: 450 N. Orientation of sensor axes, x-tilt, +TX, y-tilt, +TY and vertical acceleration, +AZ is shown

the base plate, houses the tilt and acceleration sensor. The larger titanium case that lies horizontally in a plastic tray contains the data logger, electronics and batteries. Underwater connectors in the end caps of both pressure cases feed the analog sensor signals from the aluminium pressure case into the titanium case, which houses the data logger. A newly developed analogue deep sea level (Fabian and Heesemann 2006) adjusts the instrument by means of an ROV.

Sensors

The OBT has two main sensors: A biaxial bubble tilt sensor and an absolute accelerometer that has a response curve starting from DC. In addition, a thermistor incorporated in the tilt sensor measures the temperature inside the sensor pressure case, whereas the bottom water temperature is recorded with a miniaturized high-resolution (1 mK) temperature logger (Pfender and Villinger 2002), which is lashed to the frame of the OBT.

Tilt

We use an Applied Geomechanics Inc. (AGI) 756 wide angle biaxial bubble tilt sensor with a resolution of 1.0μ rad (0.2 arc second) and a repeatability of 2.0μ rad (AGI 2000). This type of sensor is known for its reliability and long-term stability (d'Orey de Lantremange 1998; Mentes et al. 1996; Tofani and Horath 1990). The comparatively broad effective range of ±8° is particularly useful for our application. Hence, we do not need to level the sensor (or the frame) very precisely when installing it with an ROV on the sea floor.

Compared with data of Tolstoy et al. (1998, 2002), who used a 0.05μ rad resolution tilt sensor within an OBS with a gimbal system, and assuming the same sea floor conditions, we can clearly resolve long-term signals with high quality. Tolstoy et al. (1998) also report tidal related tilts of amplitude below 1.0μ rad. However, the signal strength depends on the sea floor compliance and is position-dependent (Willoughby et al. 2000; Crawford 2004; Hulme et al. 2005). Therefore, we can not exclude the possibility that we will observe tide-related tilt in the Logatchev hydrothermal vent field.

The tilt sensor electronics include a signal conditioning card with two switchable gains of ratio 10 (high) to 1 (low) (AGI 2003). High gain amplifies small tilt signals within a reduced effective range of ±0.8°. For OBT operation we use the low gain setting and feed the signals into a 24-bit data logger, so that a final signal resolution of better than 1.0μ rad is achieved.

The signal conditioning card also has a built-in switchable low-pass Butterworth filter with cut-off periods of 0.05 s and 7.5 s both with 6 dB/octave roll-off. For OBT operation we use the 7.5 s setting to reduce aliasing.

An other criterion for sensor selection is the power consumption. Our AGI 756 with signal conditioning card needs about 15 mA at ±12 V at an inclination smaller than 2°. The AGI 756 also needs up to 27 mA for larger angles in both axes. If the sensor is leveled almost exactly then the required current drops to 11 mA. For autonomous long-term monitoring it is desirable to reduce these values further in the future. However, presently there are no sensors now on the marked with similar resolution, repeatability, long-term stability and significantly less power consumption than the AGI 756.

Acceleration

For measurement of vertical acceleration we choose the Kistler Servo K-Beam 8330A2.5 (Kistler 2004). This is a MEMS class sensor, which is already used in reflection seismic surveys (Byerley et al. 2003) and also is suitable for seismological applications (Holland 2003). Micro-Electro-Mechanical Systems (MEMS) integrate mechanical elements as well as sensor elements and electronics on a single small silicon wafer. Similar to computer processor fabrication, the MEMS sensor is fabricated through micro fabrication. Due to the small size and high fabrication precision, these sensors consume only a fraction of the power used by a comparable classical sensor. Therefore, the MEMS sensors noise level is relatively low and the resolution as well as accuracy is quite high (Bernstein et al. 1999; Hierold 2004; Moore and Syms 1999; Mougenot and Thorburn 2004; Varadan 2000).

Nominal signal resolution of the Servo K-Beam is close to 10^{-5}m/s^2 with a sensitivity of about 150 mV/(m/s^2). Frequency range is from DC to 300 Hz (resonance frequency is 5000 Hz). To reject high frequency components, which can not be sampled by our data acquisition system due to power limitations, we connected the output of the sensor to a passive low-pass filter with 1 Hz corner frequency and a roll-off of 18 dB/decade.

As mentioned above, the strength of low frequency background noise on the sea floor is in the same range as the resolution of the Servo K-Beam (Crawford and Webb 2000; Duennebier and Sutton 1995; Romanowicz et al. 1998; Zverev 1997), so that the sensor's resolution is sufficient for monitoring seismicity level. For long-term deep sea measurements the MEMS sensor has several advantages. Compared to a classical seismograph these are small physical dimensions (27 × 27 × 16 mm), operation without precise leveling, relatively low power consumption (≈17 mA, ±12 V), robustness against mechanical shocks during transport and deployment, low cost, light weight and easy handling.

The Servo K-Beam works in any orientation. It measures absolute acceleration in the direction of the sensor axis (here in the vertical instrument axis of the OBT). Because of this particular capability to measure gravity, the combination of long-term acceleration and tilt helps to verify long-term trends. Significant changes in tilt have to be accompanied by a deviation of the OBT, and as well by a comparable change in absolute acceleration. On the other hand, with tilt data, vertical acceleration can be corrected for deflections (Crawford and Webb 2000).

Recently, Kistler Corporation has replaced the Servo K-Beam 8330A2.5 by its successor the Servo K-Beam 8330A3.0. With respect to the 8330A2.5, the nominal noise density of the 8330A3.0 decreased by 50% and the nominal resolution is enhanced by the same factor. The measuring range is 20% broader and the sensitivity is reduced by about 20%. The temperature coefficient has been increased by a factor of nearly four. Minor modifications concern the frequency range, resonant frequency and the phase-shift (Kistler 2004, 2005). However, the test data we show in section 'Tests' from both sensors, does not report large differences between the sensors in practical operation.

Data logger and low power operation

The data logger has to fulfill several requirements, which are (1) a suitable number of input channels with a sufficiently high dynamic range and a sampling interval small enough to resolve signals related to seismicity, (2) storage capacity for at least one year of data, (3) low power consumption and, (4) small size and low cost. The battery capacity and the memory size of the data logger have to be designed for a one year long monitoring period at the sampling intervals described below.

The Oceanographic Embedded Systems AD 24 24 bit AD-converter controlled by a Persistor Instruments Inc. CF 2 (PersistorInc 2005) is a data logging system, whose technical specifications meet our requirements. The AD 24 is an add-on module that can be plugged in the CF 2's upgrade socket. The AD 24 implements two Cirrus Logic Inc. CS 5534-BS 24 bit Sigma-Delta converters, which provide four multiplexed input channels each. Each of the channels can be configured freely.

The CF 2 is a Motorolla 68332 based embedded computer system with 1 MB RAM and a slot for CompactFlash cards. During logging, the RAM can be used as a data buffer whose content is dumped to the CompactFlash card when the buffer is full. The AD 24 board and CF 2 controller come with a suite of C-libraries. Customers can incorporate functions of the C-libraries in their own C-Code and build a customized acquisition and processing software package.

The most important settings for an input channel of the AD 24 are the conversion time, which is directly related to the resolution, and the sampling period, which has to be longer than the conversion time. At a conversion time of 600 ms, a resolution of 22 effective bits for an input signal of ±2.5 V can be achieved, but the resolution depends somewhat on the individual Sigma-Delta chip. Conversion time must be reduced, if the sampling period is reduced to a time equal or shorter than the conversion time. Accordingly, the effective resolution is reduced. On the other hand, if the highest resolution is not necessary (e.g., because of limited sensor resolution), one can configure the corresponding channel to run at a shorter conversion time, even if the sampling period is much longer. The remaining time between sampling period and conversion time can be used for dumping the content of the data buffer from the RAM to the CompactFlash card, or it can be used for switching the AD 24 and/or the CF 2 to its power saving mode. The latter is a very advantageous setting for autonomous long-term operation.

In the standard OBT settings one channel is configured to log the acceleration sensor output (i.e., output behind the low-pass filter) every 750 ms. To achieve 21 effective bits resolution, which corresponds to the sensors resolution, we set the conversion time to 300 ms. Therefore, every 750 ms, a period of 300 ms is used to convert the acceleration values. The remaining 450 ms are used to sample tilt (x-tilt, y-tilt) and internal temperature, to dump the data buffer to the CompactFlash card, or to switch the data logger to sleep mode. To determine both digital tilt values a 200 ms conversion time, corresponding to 19 bit effective resolution, is used. A 30 ms conversion time, which corresponds to an effective resolution of 17 bit, is applied for the internal temperature. Again, these settings match the sensor's dynamic ranges.

A timing diagram of one sampling cycle in standard settings is shown in Fig. 2. The cycle is implemented in the acquisition software as a loop. Eight individual tasks of the data logger are executed in a sequence of eight periods within this loop. Every task is controlled by the real time clock of the CF 2. The clock is also used to record a time stamp for the first data point of every cycle. Clock drift measured during laboratory tests with two different CF 2's is about + 0.5 s/day at room temperature (20–23°C). The time stamp is determined at the beginning of every loop/sampling cycle and parallel to the conversion of the first acceleration value. This moment is denoted by 'DATE+-TIME' in Fig. 2. The eight individual tasks are: (1) take acceleration data (AZ) – sleep (2) take acceleration data (AZ) – take x-tilt data (TX) – sleep (3) take acceleration data (AZ) – take y-tilt data (TY) – sleep (4) take acceleration data (AZ) – take temperature data (T_{int}) – sleep (5) take acceleration data (AZ) – sleep (6) take acceleration data (AZ) – sleep (7) take acceleration data (AZ) – sleep (8) take acceleration data(AZ) – dump data to the buffer(BUFF)/CompactFlash card(CF-CARD) or sleep. Because the sampling period of acceleration data is 750 ms the loop repeats every 6000 ms, which is the sampling period for tilt and temperature data. The loop runs until the CompactFlash card is full.

With these settings the data logger (AD 24 and CF 2) has a mean current consumption of 15 mA that is independent from the operation voltage of the logger, which should always be between 3.3 V and 15 V. For power saving on the one hand and endurance of operation on the other we chose a battery supply with 7.5 V output, deliberately not too close to the threshold values.

At maximum inclination (≥ 8° in both directions TX, TY) the maximum power consumption of all OBT components is about 641 mW, which decreases to 497 mW at a mean inclination below 2° and is minimal at 449 mW. With a safety factor of two the battery pack of the OBT is budgeted to power the instrument for 269 days (maximum power consumption), over 332 days (mean power consumption) to 367 days (minimum power consumption). We use a 512 MB CompactFlash card that can store data from more than 600 days of standard OBT operation.

Ground coupling, leveling devices and the frame

Good coupling of the sensor to the ground is very important for tilt and low frequency acceleration measurements (Agnew 1986). Therefore, there are no moving parts between the sensors and the contact points of the tripod on the ground. For platform tiltmeters like the OBT, the best possible coupling should be attained. A pure passive gimbal leveling system, for instance, needs additional mechanical components, which itself needs a thorough mechanical design and testing procedure. Moreover, actions of the gimbal

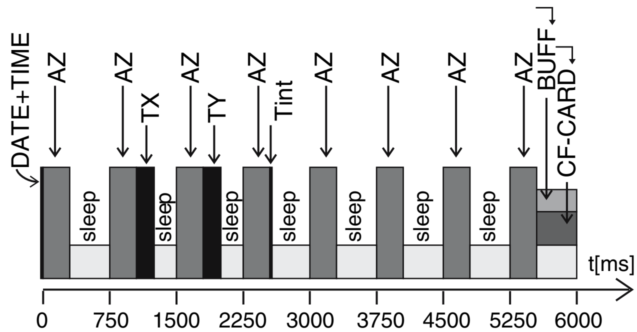

Fig. 2 Timing diagram for a sampling-cycle of the OBT in standard settings. Time t is denoted in ms on the horizontal axis, which is divided in eight periods of 750 *ms*. Within each period, data is taken and converted. The thin line in black, which is labeled with 'DATE+TIME,' and which is drawn before the cycle, indicates the reading of the real-time clock of the microprocessor of the data-logger. This is done independently from the other tasks of data conversion. The dark-grey segments, which are labeled with 'AZ', indicate conversion-time of acceleration data. Shorter black segments, which are labeled with 'TX', 'TY' and 'T_{int}', display conversion-times of tilt and temperature values, respectively. The width of these grey segments, i.e., conversion-time, is related to the resolution, at which the data is converted. Power saving is active during the times, which are depicted in light-grey and labeled with 'sleep.' The only exception is during the eighths period, between 5250 *ms* and 6000 *ms*. Besides power saving, data can be written to a buffer (see the arrow labeled by 'BUFF'), or, if the buffer is filled up, the data can be written from the buffer to the CompactFlash card (see the arrow labeled by 'CF-CARD')

system during operation have to be logged with tilt and acceleration data. This in turn would require additional memory and power capacity. In constructing a robust, easy to handle tool for long-term monitoring we decided not to use moving components. The consequence is that the tilt resolution is decreased, because the available tilt sensor has to have a comparatively broad measurement range. The benefit is that only approximate leveling of the OBT with the ROV is required.

The frame of the OBT comprises two main parts. The first part consists of the base plate with legs, sensor pressure case, deep sea level and frame for handling (Fig. 1). These components, except the glass sphere of the deep sea level, are of massive sea water resistant aluminium. The use of light weight aluminium instead of stainless steel or titanium is dictated by the maximum pay load of the ROV manipulator arm, which is limited to about 500 N in water. A light weight instrument is also easy to handle on-board a vessel. However, we constructed the OBT to have a large mass (i.e., equivalent to the pay load of the ROV arm) and a small and compact shape. A massive instrument of compact size is assumed to have better ground coupling. Due to its large mass, such an instrument is less sensitive towards disturbing forces, while its compact shape results in a only minor drag to near sea floor currents. Tiny movements of the instrument, which loosens the contact between the OBT's legs and the subsoil, are thus reduced. The legs have a hollow profile on their tips, which should reduce settling of the instrument under its own load. All parts are fixed with aluminium screws (instead of steel or titanium) to prevent electro-chemical processes between different metals. The sensor pressure tube and the glass sphere of the deep sea level are rated to full ocean depth. The deep sea level (Fabian and Heesemann 2006) houses a circular spirit level with a gas bubble that can be viewed through the glass sphere by the ROV camera. This allows manual adjustment of the instrument leveling by the ROV. Additionally, two mercury electronic levels are included and switch light-emitting diodes (LED), which signal when leveling is better than 5° and 2° respectively.

The second part of the frame consists of the large titanium pressure tube that contains the electronics, batteries and data. The titanium pressure cylinder contracts during lowering of the OBT to the ocean floor and causes a deformation signal. Therefore, this cylinder is mechanically (and electro-chemically) isolated from the base plate and the rest of the frame by a deformable plastic tray. To prevent electro-chemical reactions between titanium and aluminium additional Zinc anodes are attached to the frame.

Tests

We tested the sensors and data acquisition electronics of the OBT at the University of Bremen. The sensors were screwed next to one another on a small metal base plate, which itself was placed on top of a massive metal workbench. The laboratory is located on the fourth floor of a five storey building. Tests were concentrated on long-term stability and reliability of the data acquisition system.

For a long-term test over 40 days we set-up the data logger to run faster, i.e., to sample acceleration at a period of 400 ms, instead of the 750 ms in standard OBT settings as described above in section 'Data logger and low power operation'. Accordingly, tilt and sensor temperature are sampled every 3200 ms. Due to these settings, signal resolution decreased and power consumption was increased. The same sensors that were later included in the OBT, i.e., the Kistler Corp. Servo K-Beam 8330A2.5 accelerometer and the AGI 756 biaxial tilt sensor with thermistor, were used in the laboratory. Instead of batteries we used a power supply. Acceleration data AZ shows high noise levels of about 1 mm/s^2, which is about to 50 times stronger than the resolution of the acceleration measurements at the conversion time of 200 ms. Compared to this, noise level in tilt data TY, TX has an amplitude of about 10μrad, i.e., nearly five times the resolution, which can be achieved at the used settings of 100 ms conversion time.

Figure 3 shows the data recorded from 15th December 2004 to 24th January 2005. Measurements were started on 14th December, but we excluded data from the first 24 h, because there were disturbances in the acceleration record, caused by laboratory work, and a settling of about 95μrad in both tilt components. The filtered time-series of acceleration data AZ shows that spike-like events on 1st, 7th and 13th of January are disturbances that contain only high frequencies. Apart from the short period noise, the acceleration signals strongly correlate with the internal sensor temperature, T_{int}. In particular, during phases when the temperature fluctuated strongly, e.g., on 15th, 16th, 21st, 24th, 25th, 29th December or during the 6th and the 21st, 22nd and 23rd January the correlation between T_{int} and the vertical acceleration AZ is quite strong. On 21st December this correlation was somewhat weak, and it reduced further on 11th and 12th January. A very similar relation applies to the correlation between the temperature and the tilt components. However, this picture is not uniform. For instance, on 17th, 18th, 22nd, 31st December and 4th, 7th, 10th, 12th, 15th and 17th January, the correlation between both tilt-components and temperature is rather similar and strong. In contrast, on 16th, 24th, 25th, December and on 19th January correlation with temperature is significant, but quite different between both tilt-components. A very similar correlation of acceleration with temperature and tilt with temperature is only recorded on 15th January. The reason for the strong, but quite non-uniform influence of temperature variations is most likely a complex expansion and contraction of the metal constructions of sensors, the metal base plate and the workbench.

Further remarkable features of Fig. 3 are noted on the record for the 29th December, when an increase in T_{int} seems to cause a jump in acceleration data AZ, but could additionally be biased by a change in tilt TX and TY. The strong jump in TX on the 6th January of about 75μrad is accompanied by a very small change in TY, which appears to be somewhat unusual, as well as a stronger signal in AZ. Another similar jump in TX, but about three times smaller, is seen on the 18th January. Both signals are actually gradual changes over a short time interval, but appear as jumps on the compressed time scale of Fig. 3. Generally, the signal

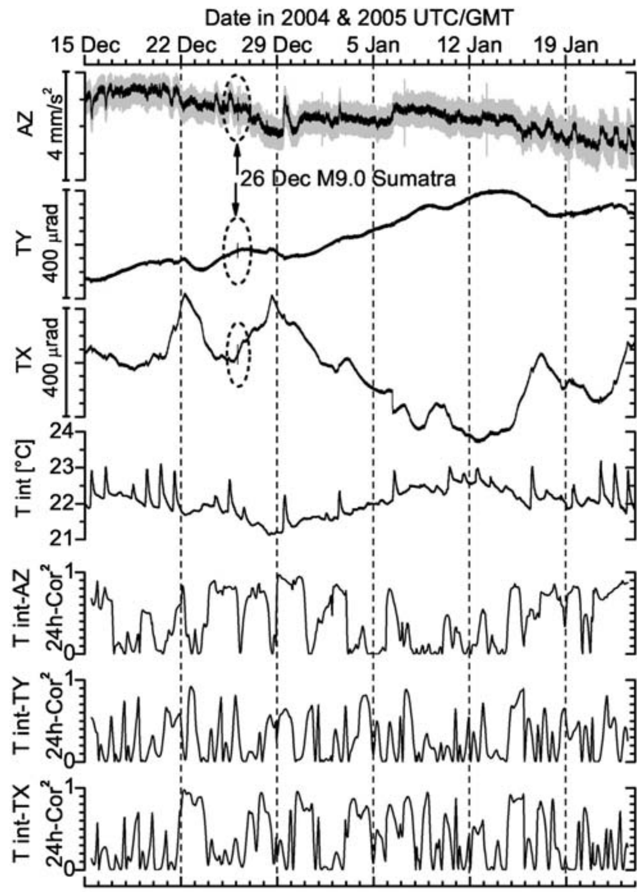

Fig. 3 Long-term test data over 40 days from December 15, 2004 until January 24, 2005 and moving-window correlation with temperature. From top to bottom the upper four time-series show: original vertical acceleration AZ (Kistler Servo K-Beam 8330A2.5) in light-grey, which is painted-over by filtered vertical acceleration in black (filter-frequency is 0.15 Hz). The diagram-panels below show the two perpendicular tilt components TY and TX and the sensor temperature, T_{int} (from AGI 756 biaxial tiltmeter with thermistor). Compare Fig. 1 for the sign and orientation of sensor axes to each other. The lower three time-series show moving-window calculations of the square of the cross-correlation between the sensor temperature T_{int} and the other data. Width of the moving-window is 24 h with a shift of 1 h between two windows. T_{int}-AZ is the correlation between the sensor temperature and the filtered acceleration data, T_{int}-TY the correlation with the Y-component of tilt, and T_{int}-TX the correlation with the X-component of tilt. On the whole, noise originating from temperature variations and most likely caused by human activity dominates the data. Nonetheless, signals, which were caused by teleseismic waves of the M9.0 Sumatra earthquake of 26th December, with a epicentral distance of 9527 km, appear in the time series of tilt and of acceleration (see also the Fig. 4 that has an enlarged view on the signals from the seismic waves)

of TY seems to be smoother than that from TX. In other test configurations we checked both tilt components, but could not determine a difference between them. The long term change in temperature T_{int} between the 29th December and 24th January seems to correlate quite well with the long term trend of TX and TY. However, the accelerometer measures absolute values, i.e., gravity, and all sensors are mounted on the same base plate. Hence, the long-term change in TY of about 250μrad over the complete time series might cause the accompanying drop in acceleration values. We note that there is no comparable change in the temperature T_{int}, which starts and ends at about 22°C. On the other hand, the strong long-period tilt variation in TX between the 22nd and 29th December and around the 17th January did not appear to be significant in the acceleration data AZ.

The teleseismic waves of the M9.0 Sumatra earthquake of 26th December are mostly buried in the broad range of signals in Fig. 3 but cause a clear signal in tilt and acceleration. Shaking of our institute building is clearly visible in tilt TX, TY, but acceleration values also rise above the ambient noise level. Details are shown in Fig. 4.

In Fig. 4 we smoothed the original acceleration data with the same digital low-pass filter that was applied to the data in Fig. 3 and that had a cut-off frequency of 0.15 Hz (6.67 s). Because of this data smoothing, noise is reduced and the seismic waves (mostly the surface waves that have their main frequency content below 0.15 Hz) appear quiet well. This proves that the Servo K-Beam MEMS accelerometer is well suited to detect motions in the frequency range between about 1 mHz and 1 Hz, and especially in the frequency range of teleseismic waves.

The amplitude spectra in the lower four panels of Fig. 4 show significant frequency components in the acceleration as well as the tilt registration. The strongest frequency components, which are caused by teleseismic waves, and which clearly correspond to the spectrum calculated from the seismological data of Bad Segeberg (BSEG-Z), are between 0.03 and 0.09 Hz. The tilt spectra also correspond to the spectrum BSEG-Z in the lower frequencies between about 0.017 and 0.03 Hz. These spectra (BSEG-Z, TY, TX) become nearly flat in the frequency range down to 1 mHz. Spectra lines of the acceleration spectrum are not so striking. The acceleration spectrum also shows increasing components in the low frequency range down to values of 1 mHz. Single spectra lines did not correspond across all spectra. For instance, a spectra line at 0.041 Hz in TY corresponds very well with the spectra line in BSEG-Z, but it does not correspond with the other spectra of AZ and TX. Different orientation of the sensors in space may explain this discrepancy.

During a second long-term test with a spare system of the OBT's sensors and data logger we recorded a

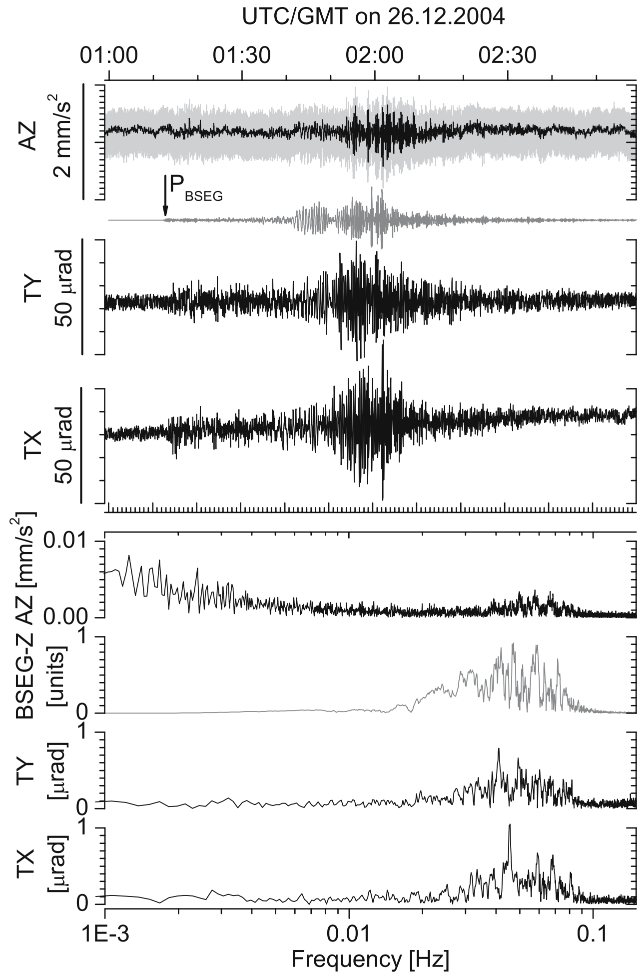

Fig. 4 Teleseismic waves of the M9.0 Sumatra earthquake of December 26, 2004, 00:59 Universal Time Coordinated (UTC/GMT), and corresponding amplitude spectra. The signals denoted by AZ were recorded with a Kistler Servo K-Beam 8330A2.5 accelerometer, and the signals denoted by TX, TY with an AGI 756 tilt sensor. Epicentral distance is 9527 km. To the comparison we included between the records AZ and TY the uncalibrated record of the vertical component of the German seismological station in the town Bad Segeberg (Henger et al. 2002), which is about 150 km northeast of our laboratory in Bremen. This record is in grey. The *p*-wave arrivals are denoted by the arrow and P_{BESG}. In all, the notation is the same as used in Fig. 3. AZ shows the original data in light-gray; over-printed data in black is filtered with a digital low-pass filter with 0.15 Hz cut-off frequency. Both TX and TY show original and unfiltered data. The lower four panels of the diagram show the amplitude spectra. The spectra of the vertical acceleration AZ is calculated from the filtered data

second teleseismic event. The logger was set up to run in OBT standard mode (see section 'Data logger and low power operation'). As in the first test (Figs. 3, 4) the recording system worked very reliable, in this case for over two months, and produced time series of quite similar quality. In this test we changed the accelerometer type and tested the new Kistler Servo K-Beam

8330A3.0. The data shown in Fig. 5 confirms that this new sensor is also appropriate for our application. The teleseismic waves of the M7.6 Pakistan earthquake of 8th October 2005 (BGR 2004a) appear clearly. At a first glance, wave form data from our sensors is not as obvious as in Fig. 4. Inspected more precisely and compared with the recordings of the seismological station in Bad Segeberg (northern Germany; (Henger et al. 2002)) the event becomes obvious. However, energy release of this earthquake is several times smaller than of the M9.0 Sumatra, even if epicentral distance is roughly halved. For this test we used another tilt sensor (but of the same AGI 756 type) compared to the former test shown in Fig. 4. The difference in the noise level of tilt before and after the teleseismic waves in Figs. 4 and 5 are due to the better resolution of the data logger, which was switched to the OBT standard mode.

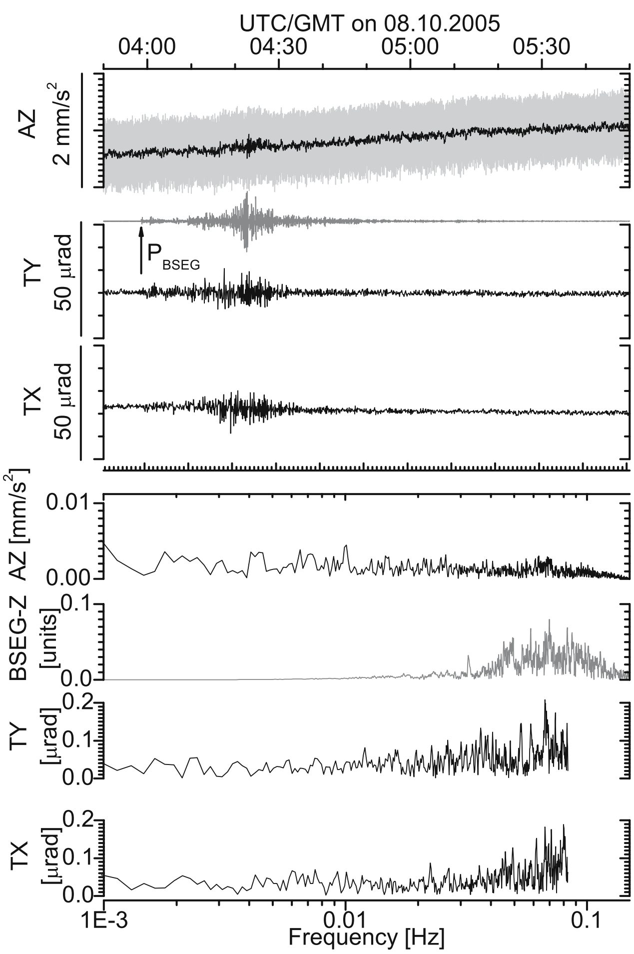

Fig. 5 Teleseismic waves of the M7.6 Pakistan earthquake of October 8, 2005, 03:50 Universal Time Coordinated (UTC/GMT) (BGR 2004a), and corresponding amplitude spectra. The representation is as in Fig. 4. Here, the signals denoted by AZ were recorded with a Kistler Servo K-Beam 8330A3.0 accelerometer, and the signals denoted by TX, TY with an AGI 756 tilt sensor. Epicentral distance is 5364 km. Again, for a better identification of the seismic waves we added (in grey) the uncalibrated record of the vertical component of the German seismological station in Bad Segeberg, which is about 150 km northeast of Bremen. The *p*-wave arrivals are denoted by an arrow and P_{BESG}. TX and TY show original data

The amplitude spectra of acceleration AZ and tilt data TY, TX as well as of the seismological data from Bad Segeberg, BSEG-Z are depicted in the lower four panels of Fig. 5. Due to the lower sampling period (6000 ms), the spectra of tilt data are limited to 0.083 Hz. Compared with the data shown in Fig. 4, amplitudes of BSEG-Z are now nearly ten times smaller and amplitudes of TY and TX are about five times smaller. In both Figs. 4 and 5, the spectra of acceleration data have the same scaling. In accordance with the smaller energy release of the Pakistan earthquake, the frequency components in the spectrum of acceleration are weak and significantly appear only between 0.06 and 0.071 Hz. In the low frequencies down to 1 mHz the spectrum does not show a gradual increase of amplitudes, as seen in Fig. 4, but has some relatively prominent lines, e.g., 0.01 or 0.0043 Hz. Due to disturbances from the laboratory surroundings, high frequency noise, which can be seen in the time series as the broad grey band, is about 40% stronger than in Fig. 4. Under these circumstances, it is hard to quantitatively compare both acceleration sensors, but we can conclude that both are suited for the OBT.

A further demonstration of the capability and the suitability of the OBT's sensor system is shown in Fig. 6. During a short term test of the measuring system we observed seismic signals from a local earthquake. On October 20, 2004 a M4.5 local earthquake occurred about 45 km southeast of Bremen. Source time of the event was 06:59 Universal Time Coordinated (UTC/GMT) (BGR 2004b). The earthquake had an intensity of V+ on the European Macroseismic Scale and was felt in the Bremen geoscience institute building by some colleagues. In this case too, we used the Kistler Servo K-Beam 8330A2.5 MEMS sensor to measure vertical acceleration together with the AGI 756 tilt sensor, which were both used in the OBT. The data logger was set-up to log each of the sensors with the highest resolution, i.e. with a conversion time of 600 ms. Sampling interval was 8 s. The crosses on the time series in Fig. 6a indicate single data points. The tilt sensor clearly observed the shaking of the institute building. Because the accelerometer output was logged with the long sampling interval and because the local earthquake did not generate a significant amount of low-frequency accelerations, only a single pulse can be seen in the corresponding data. The motion sequence

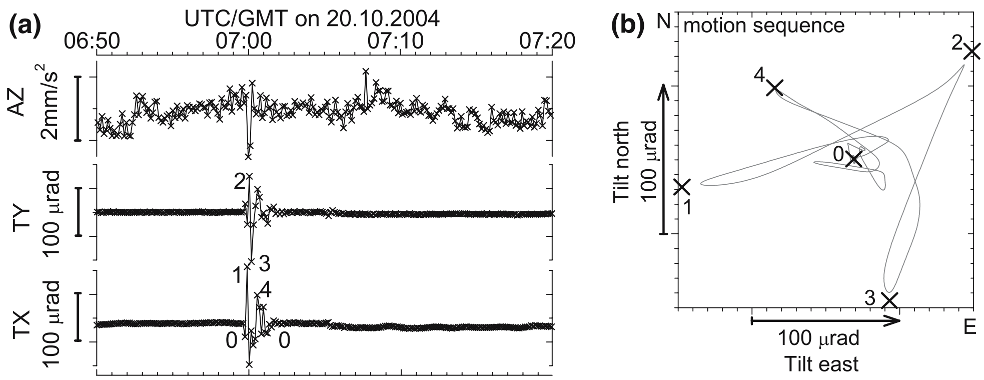

Fig. 6 Signals from a near earthquake (**a**) with hodograph (**b**). (**a**): Signals caused by the M4.5 local earthquake in the town Rotenburg/Wümme, which is about 45 km away from Bremen. The earthquake appeared on October 20, 2004, 06:59 Universal Time Coordinated (UTC/GMT). Notation is like in Figs. 3, 4 and 5. Sampling interval is 8 s. Data points are marked by crosses. The tilt sensor (TX, TY) recorded highly significant signals. The Kistler Servo K-Beam 8330A2.5 acceleration sensor recorded a single pulse that just rises above the noise level of about 1 mm/s^2. (**b**): Hodograph drawn by a B-spline interpolation from the tilt data TX, TY. The numbered positions in the hodograph correspond with the numbered times in part (**a**). The hodograph is oriented towards north

of the tilt sensor is illustrated by the hodograph in Fig. 6b, within which the tilt in northern direction is plotted against the tilt in an easterly direction. The numbers and crosses correspond with the numbered crosses in Fig. 6a. The hodograph is drawn through a B-spline interpolation between the data-points. In any case, a consistent direction of deflection, which is related to the direction of the epicenter, cannot be recognized. Similarly we analyzed the data displayed in Figs. 4 and 5 by means of hodographs, but also could not find a consistent direction of deflection.

In summary, sensors and data acquisition system work reliable, but the test data shows a lot of interfering signals, which result from temperature variations and most likely from seismic noise, shaking of the institute building or man-made electro-magnetic noise. The geological setting in the region of Bremen in northern Germany is characterized by a thick sedimentary column of several tens to thousands of meters thickness, overlying crystalline basement (Hennigsen and Katzung 1998) and favors anthropogenic-induced micro seismicity (Ibs von Seht 1999). Environmental conditions in our laboratory onshore are quite different from those predicted on the deep sea floor. The greatest differences are that temperature on the deep sea floor is very stable and that electro-magnetic and anthropogenic noise is absent. Indeed, on the deep sea floor, as found at the Logatchev hydrothermal vent field, in about 3000 m depth, temperature ranges to within 0.1 K at nearly 2°C (Davis et al. 2003). Moreover, due to the electro-magnetic shielding and the skin effect in sea water, nearly no electro-magnetic noise is expected in these large water depths (Greiner 1991). Weaker signals than the signals which we recorded in the tests, or tremor-like events can not be observed in our laboratory. Generally, for this purpose the level of disturbances appearing in the test data has to be reduced and the sensors have to be placed closer to the signal source. Compared our Bremen laboratory, the sediment cover in the Logatchev hydrothermal vent field is interrupted by outcropping basement. Sediment layers are much thinner, rarely exceeding more than one or two meters (Kuhn et al. 2004; Lackschewitz et al. 2005). As a result there should be no surface waveguide to generate strong interfering ground motions. Furthermore, in the Logatchev hydrothermal vent field the OBT would be close to earthquakes on the Mid-Atlantic Ridge. These environmental conditions are all very helpful to our goal of achieving high-resolution measurements with the OBT.

Deployment

During cruise M64/2 (May 2005) of research vessel 'Meteor' the OBT was deployed using the ROV 'Quest' of the MARUM Institute, University of Bremen (Lackschewitz et al. 2005). The instrument was placed on a central position in the Logatchev hydrothermal vent field. The deployment coordinates are 14°, 45.201′ N; 44°, 58.784′ W; 3053 m depth, Fig. 7. The position is southeast of site 'Quest' and west of site 'Irina II'. Two assumed tectonic faults pass close by the OBT position (Kuhn et al. 2004). The site of the OBT is far enough from vent sites so that measurements are not thermally influenced by hot fluids.

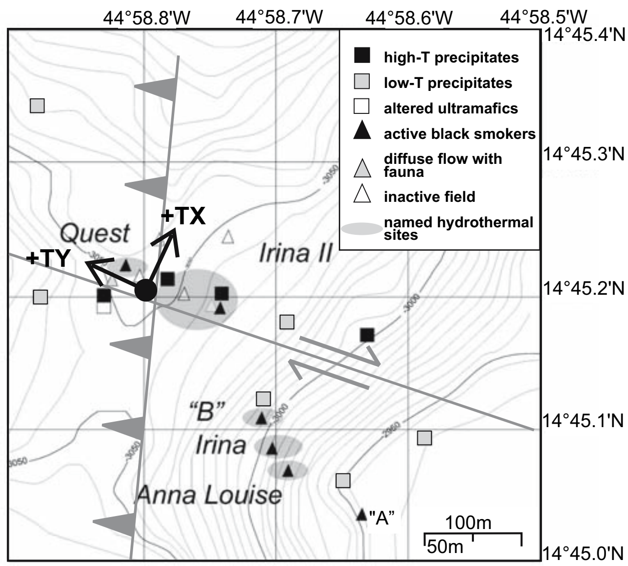

Fig. 7 Map of the Logatchev hydrothermal vent field modified after Kuhn et al. (2004). The black point with arrows, which are labeled with '+TY' and '+TX,' display the position and axes orientation of the OBT. The topography (ocean depth), special features of the site, such as black smokers and two assumed tectonic faults are printed in the background. The axis of the Mid-Atlantic Ridge is in western direction

The entire Logatchev hydrothermal vent field is mostly characterized by steep slopes of a few meters elevation separating small sediment covered plateaus. Small piles of brittle rock from the basement rise above the sediment cover. The OBT was installed on the top of a small rock pile (Fig. 8) and was levelled to within 2° by firmly and carefully pressing and moving the legs of the instrument with the manipulator arm of the ROV. The floating rope seen in Fig. 8 was attached above the center of mass of the OBT and was required by the ROV team for deployment. It adds less than 1 N buoyancy to the 450 N OBT. The rope may move in bottom currents, but is assumed to have a negligible effect on the measurements. The types of rock piles seen in Fig. 8 are the most stable sea floor available in this area. Bare rock surface could not be found in the Logatchev hydrothermal vent field. Inspection of the OBT during a re-visit with the ROV 5 days after deployment showed that leveling of the OBT was still sufficient. Therefore, we assumed that the OBT has a stable location and good coupling to the ground. Orientation of the OBT was determined from the compass of the ROV by looking twice with the ROV in the direction of one of the OBT's axes. Orientation of the +TY-axis is 295°±3° clockwise from north and of the +TX-axis 25°±3° clockwise from north (cf., Fig. 7).

Fig. 8 The OBT in the Logatchev hydrothermal vent field on top of a small rock pile. For installation with the ROV a floating rope was tied on the OBT above the center of mass. On the left side of the OBT frame an additional aluminium L-profil holds a miniaturized temperature logger. Steep slopes (here in the foreground of the photo) and a sediment cover of about 1 m thickness (here in the background) characterize the area. Ripples on the sea-floor in the background indicate currents

Summary

The OBT was developed to monitor seafloor deformation and acceleration, with the goal of observing signals, caused by hydrothermal activity, fluid discharge from the upper crust, seismicity level, and the coupling of those processes within the Logatchev hydrothermal vent field. We constructed a robust, easy to handle scientific tool called the OBT from as few components as possible. Deployment of the OBT is performed by means of an ROV. Hence, we were able to omit moving parts, such as automatic leveling devices for sensors or frame. A tilt sensor of type 756 from Applied Geomechanics Inc., which has a resolution of 1.0μ rad and a broad range of ±8°, has a sufficient dynamic range for our scientific goal. To detect vertical acceleration we employed a MEMS accelerometer of type Kistler Corp. Servo K-Beam 8330A2.5. The MEMS accelerometers turned out to be well suited to observe seismicity levels below 1 Hz. In laboratory tests the sensors detected teleseismic waves from distant earthquakes and also recorded signals from a relatively local event. For low power data logging we implemented a Persistor Inc. CF 2 with an AD 24 analog to digital converter. We developed data logging software for the CF 2 that allows us to acquire high resolution long-term data with very low power consumption, resulting in the possibility of long-term monitoring over one year or longer. During cruise M64/2 of RV 'Meteor' in May 2005 the ROV 'Quest' of the MARUM Institute, University of Bremen installed the OBT at a central position in the Logatchev hydrothermal vent field, Mid-Atlantic Ridge. The first data are expected by the middle 2007, and will be published in subsequent articles.

Acknowledgements We thank the German Research Foundation (Deutsche Forschungsgesellschaft, DFG) for support of our investigations in the frame of Priority Program (Schwerpunktprogramm, SPP) 1144. Our engineer B. Heesemann is acknowledged for implementation of the OBT design and the design of the deep sea spirit level. E. Lippmann assisted in the design of electronic components. We thank P. D. Clift and three anonymous colleagues, which made useful comments to improve the manuscript. The captain and the crew of RV Meteor and the MARUM ROV Team of University of Bremen is acknowledged for deployment of the OBT. The photo of the OBT in the Logatchev hydrothermal vent field was provided by MARUM, University of Bremen. Wave form data from the seismological station in Bad Segeberg is available via the WWW-site of Seismologisches Zentralobservatorium Gräfenberg (SZGRF).

References

AGI (2000) User's manual no. B-92-1003, rev. B., series 755, 756 and 757 miniature tilt sensors, Applied Geomechanics Inc., Santa Cruz, CA 95062 (USA), http://www.geomechanics.com/

AGI (2003) User's manual no. B-92-1002, rev. D., model 83162 dual-channel signal conditioning card, Applied Geomechanics Inc., Santa Cruz, CA 95062 (USA), http://www.geomechanics.com/

Agnew DC (1986) Strainmeters and tiltmeters. Rev Geophysics 24(3):579–624

Anderson G, Constable S, Staudigel H, Wyatt FK (1997) A seafloor long-baseline tiltmeter. J Geophys Res 102(B9):20269–20285

Bernstein J, Miller R, Kelly W, Ward P (1999) Low-noise MEMS vibration sensor for geophysical applications. J Microelectromech Syst 8(4):433–438

BGR (2004a) Erdbeben, Besondere Ereignisse, Seismic Data Analysis Center, http://sdac.hannover.bgr.de/web/sdac/beben/erdbeben.html

BGR (2004b) Ursache des Erdbebens von Rotenburg/Wümme aufgeklärt, Pressemitteilung 3.12.2004, Bundesanstalt für Geowissenschaften und Rohstoffe, Stilleweg 2, 30655 Hannover: 2

Bialas J, Flueh ER (1999) Ocean bottom seismometers. Sea Technol 40(4):41–46

Bilham RG, Beavan RJ (1979) Strains and tilts on crustal blocks. Tectonophysics 52:121–138

Byerley G, Klausen CK, Tessman DJ (2003) EKOFISK Vector-Seis Test – Improvements in vector fidelity of 4C seismic data. In EAGE 65th Conference & Exhibition – Stavanger, Norway, 2–5 June 2003, 4

Campbell J, Kümpel H-J, Fabian M, Fischer D, Görres B, Keysers CJ, Lehmann K (2002) Recent movement patterns of the Lower Rhine Embayment from tilt, gravity and GPS data. Netherlands J Geosciences/Geologie en Mijnbouw 81(2):223–230

Chadwell CD, Hildebrand JA, Spiess FN, Morton JL, Mormark WR, Reiss CA (1999) No spreading across the southern Juan De Fuca Ridge axial cleft during 1994–1996. Geophys Res Lett 26(16):2525–2528

Chadwick WW, Embley RW, Milburn HB, Meinig C, Stapp M (1999) Evidence for deformation associated with the 1998 eruption of Axial Volcano, Juan De Fuca Ridge, from acoustic extensometer measurements. Geophys Res Lett 26(23):3441–3444

Chadwick WW, Nooner SL, Zumberge MA, Embley RW, Fox CG (2006) Vertical deformation monitoring at Axial Seamount since its 1998 eruption using deep-sea pressure sensors. J Volcanol Geothermal Res 150:313–327

Chouet BA (1996) Long-period volcano seismicity: its source and use in eruption forecasting. Nature 380:309–316

Cooper MJ, Elderfield H (2000) Diffuse hydrothermal fluids from Lucky Strike hydrothermal vent field: evidence for a shallow conductively heated system. J Geophys Res B8:19369–19375

Crawford WC (2004) The sensitivity of seafloor compliance measurements to sub-basalt sediments. Geophys J Int 157:1130–1145

Crawford WC, Webb SC (2000) Identifying and removing tilt noise from low-frequency (< 0.1 Hz) seafloor vertical seismic data. Bull Seismol Soc Am 90(4):952–963

Crone TJ, Wilcock WSD (2005) Modeling the effects of tidal loading on mid-ocean ridge hydrothermal systems, Geochemistry Geophysics Geosystems – G3. An Electronic J Earth Sciences 6(7):25, ISSN 1525–2027

Davis E, Becker K (1999) Tidal pumping of fluids within and from the oceanic crust: new observations and opportunities for sampling the crustal hydrosphere. Earth Planet Sci Lett 172:141–149

Davis EE, Wang K, Becker K, Thomson RE, Yashayaev I (2003) Deep-ocean temperature variations and implications for errors in seafloor heat flow determinations. J Geophys Res B: Solid Earth 108(1):2034–2039

d'Orey de Lantremange N (1998) Qualification test of the dual-axis bubble-type resistive tiltmeter (AGI-700 series): earth tides recorded and analyzed in the underground laboratory of Walferdange, Marée Terrestres. Bulletin d'Informations 129:9953–9962

Duennebier FK, Sutton GH (1995) Fidelity of ocean bottom seismic observations. Mar Geophys Res 17:535–555

Eberhart GL, Rona PA, Honnorez J (1988) Geologic controls of hydrothermal activity in the Mid-Atlantic Ridge rift valley: tectonics and volcanics. Mar Geophys Res 10:233–259

Fabian M (2004) Near surface tilt and pore pressure changes induced by pumping in multi-layered poroelastic half-spaces, no. 229 in Berichte aus dem Fachbereich Geowissenschaften, ISSN: 0931-0800, Universität Bremen, diss. thesis, Math.-Nat. Fak., Univ. Bonn, URN: http://nbn-resolving.de/urn:nbn:de:hbz:5-03724, URL: http://hss.ulb.uni-bonn.de/diss_online/math_nat_fak/2004/fabian_marcus

Fabian M, Heesemann B (2006) Neigungswaage für Unterwasser- und Hochdruckanwendungen (deep sea level), Deutsches Patent- und Markenamt, dE-Gebrauchsmuster (german registered design) Nr.: 20 2006 013 066.7, Universtät Bremen

Fabian M, Kümpel H-J (2003) Poroelasticity: observations of anomalous near surface tilt induced by ground water pumping. J Hydrol 281(3):191–209

Fisher AT, Zwart G, Ocean Drilling Program Leg 156 Scientific Party (1996) Relation between permeability and effective stress along a plate-boundary fault, Barbados accretionary complex. Geology 24(4):307–310

Fornari DJ, Shank T, Damm KLV, Gregg TKP, Lilley M, Levai G, Bray A, Haymon RM, Perfit MR, Lutz R (1998) Time-series temperature measurements at high-temperature hydrothermal vents, East Pacific Rise 9°49′–51′ N: evidence

for monitoring a crustal cracking event. Earth Planet Sci Lett 160:419–431
Fox CG (1999) In situ ground deformation measurements from the summit of Axial Volcano during the 1998 volcanic episode. Geophys Res Lett 26(23):3437–3440
Gagnon K, Chadwell D, Spiess FN (2005) Evolving method to measure seafloor plate tectonic motions. Sea Technol 46(7):49–52
German CR, Parson LM (1998) Distributions of hydrothermal activity along the Mid-Atlantic Ridge: interplay of magmatic and tectonic controls. Earth Planet Sci Lett 160:327–341
Goto S, Kinoshita M, Matsubayashi O, Von Herzen RP (2002) Geothermal constrains on the hydrological regime of the TAG active hydrothermal mound, inferred from long-term monitoring. Earth Planet Sci Lett 203:149–163
Greiner W (1991) Klassische Elektrodynamik, Theoretische Physik, Band 3, Verlag Harri Deutsch, Frankfurt a.M., Thun
Henger M, Berckhemer H, Seidl D (2002) The history of the development of the German Regional Seismic Network (GRSN). In Korn M (ed) Ten years of German Regional Seismic Network (GRSN), ISBN 3-527-27514-2, 1–8
Hennigsen D, Katzung G (1998) Einführung in die Geologie Deutschlands, Enke-Verlag, Stuttgart, 5th edn
Hierold C (2004) From micro- to nanosystems: mechanical sensors go nano. J Micromech Microeng 14:S1–S11
Holland A (2003) Earthquake data recorded by the MEMS accelerometer: field testing in Idaho. Seismol Res Lett Lett 74(1):20–26
Hulme T, Crawford WC, Singh SC (2005) The sensitivity of seafloor compliance to two-dimensional low-velocity anomalies. Geophys J Int 163:547–558
Ibs von Seht M (1999) Microtremor measurements used to map thickness of soft sediments. Bull Seismol Soc Am 89(1):250–259
Jahr T, Jentzsch G, Letz H, Sauter M (2005) Fluid injection and surface deformation at the KTB location: modelling of expected tilt effects. Geofluids 5(1):20
Kasahara J, Sato T (2001) Tidal effect on volcanic earthquakes and deep-sea hydrothermal activity revealed by ocean bottom seismometer measurements. J Geodetic Soc Japan 47(1):424–433
Kingston-Tivey M, Bradley AM, Joyce TM, Kadko D (2002) Insights into tide-related variability at seafloor hydrothermal vents from time-series temperature measurements. Earth Planet Sci Lett 202:693–707
Kistler (2004) Operating instructions K-Beam & ServoK-Beam capacitive accelerometers types 8304B(X), 8305A(X), 8310A(X)M11, 8312A(X), 8330A2.5, 8392B(X), 8393A(X), Kistler Instrument Corp., 75 John Glenn Drive, Amherst, NY 14228, USA. http://www.kistler.com/
Kistler (2005) Operating instructions K-Beam & ServoK-Beam capacitive accelerometers types 8304B(X), 8305A(X), 8310A(X)M11, 8312A(X), 8330(X), 8392B(X), 8393A(X), Kistler Instrument Corp., 75 John Glenn Drive, Amherst, NY 14228, USA. http://www.kistler.com/
Kovachev SA, Demidova TA, Son'kin A (1997) Properties of noise registered by pop-up ocean-bottom seismographs. J Atmos Oceanic Technol 14(4):883–888
Kuhn T, Alexander B, Augustin N, Birgel D, Borowski C, de Carvalho LM, Engemann G, Ertl S, Franz L, Grech C, Hekinian R, Imhoff J, Jellinek T, Klar S, Koschinsky A, Kuever J, Kulescha F, Lackschewitz K, Petersen S, Ratmeyer V, Renken J, Ruhland G, Scholten J, Schreiber K, Türkay M, Westernströer U, Zielinski F (2004) Mineralogical, geochemical and biological investigations of hydrothermal systems on the Mid-Atlantic Ridge between 14°45′ N and 15°05′ N (HYDROMAR I), Meteor Berichte 03-04, Mid-Atlantic Expedition 2004, Cruise No. 60, Leg 3, Leitstelle Meteor, Institut für Meereskunde der Universität Hamburg
Kümpel H-J, Fabian M (2003) Tilt monitoring to assess the stability of geodetic reference points in permafrost environment. Phys Chem Earth 28:1249–1256
Kümpel H-J, Lehmann K, Fabian M, Mentes G (2001) Point stability at shallow depth – experience from tilt measurements in the Lower Rhine Embayment, Germany, and implications for high resolution GPS and gravity recordings. Geophys J Int 146:699–713
Lackschewitz K, Armini M, Augustin N, Dubilier N, Edge D, Engemann G, Fabian M, Felden J, Franke P, Gärtner A, Garbe-Schönberg D, Gennerich H-H, Hüttig D, Marbler H, Meyerdierks A, Pape T, Perner M, Reuter M, Ruhland G, Schmidt K, Schott T, Schroeder M, Schroll G, Seiter C, Stecher J, Strauss H, Viehweger M, Weber S, Wenzhöfer F, Zielinski F (2005) Longterm study of hydrothermalism and biology at the Logatchev field, Mid-Atlantic Ridge at 15°N (revisit 2005) (HYDROMAR II), Meteor Berichte 05, Mid-Atlantic Expedition 2005, Cruise No. 64, Leg 2, Leitstelle Meteor, Institut für Meereskunde der Universität Hamburg, 6 May–6 June 2005, Fortaleza (Brazil) – Dakar (Senegal)
Lilley MD, Butterfield DA, Lupton JE, Olson EJ (2003) Magmatic events can produce rapid changes in hydrothermal vent chemistry. Nature 422:878–881
Mazarovich AO, Sokolov S (1998) The tectonic position of hydrothermal fields on the Mid-Atlantic Ridge. Lithol Mineral Res 33(4):391–394
McClain JS, Begnaud ML, Wright MA, Fondrk J, Damm GKV (1993) Seismicity and tremor in a submarine hydrothermal field: the northern Juan De Fuca Ridge. Geophys Res Lett 20(17):1883–1886
Mentes G, Lehmann K, Varga P, Kümpel H-J (1996) Some calibration of the Applied Geomecanics Inc. borehole tiltmeter model 722. Acta Geodaetica et Geophysica Hungarica 31:79–89
Moore DF, Syms RRA (1999) Recent developments in micromachined silicon. Electron Commun Eng J 11(6):261–270
Mougenot D, Thorburn N (2004) MEMS-based 3C accelerometers for land seismic acquisition: Is it time? The Leading Edge 23(3):246–250
PersistorInc (2005) Persistor Instruments Inc., Persistor Instruments Inc., 254-J Shore Rd, Bourne MA 02532-4104, USA, http://www.persistor.com/
Pfender M, Villinger H (2002) Miniaturized data loggers for deep sea sediment temperature gradient measurements. Mar Geol 186:557–570
Romanowicz B, Stakes D, Montagner JP, Tarits P, Uhrhammer R, Begnaud M, Stutzmann E, Pasyanos M, Karczewski J-F, Etchemendy S, Neuhauser D (1998) MOISE: a pilot experiment towards long term sea-floor geophysical observatories. Earth Planets Space 50(11–12):927–937
Savage JC, Prescott WH, Chamberlain JF, Lisowski M, Mortensen CE (1979) Geodetic tilt measurements along the San Andreas Fault in central California. Bull Seismol Soc Am 69(6):1965–1981
Shimamura H, Kanazawa T (1988) Ocean bottom tiltmeter with acoustic data retrival system implated by a submersible. Mar Geophys Res 9:237–254
Sleeman R, Haak HW, Bos MS, van Gend JJA (2000) Tidal tilt observations in the Netherlands using shallow borehole tiltmeters. Phys Chem Earth (A) 25:415–420

Sohn RA, Hildebrand JA, Webb SC, Fox CG (1995) Hydrothermal microseismicity at the meagaplume site on the southern Juan de Fuca Ridge. Bull Seismol Soc Am 85(3):775–786

Spiess FN, Chadwell CD, Hildebrand JA, Young LE Jr, Purcell GH, Dragert H (1998) Precise GPS/Acoustic positioning of seafloor reference points for tectonic studies. Phys Earth Planet Interiors 108:101–112

Suetsugu D, Shiobara H, Sugioka H, Barruol G, Schindele F, Reymond D, Bonneville A, Debayle E, Isse T, Kanazawa T, Fukao Y (2005) Probing south Pacific Mantle Plumes with ocean bottom seismographs, EOS, Transactions. Am Geophys Union 86(44):429, 435

Tofani G, Horath F (1990) Continuous tiltmeter monitoring to identify ground deformation mechanisms. Geotech News 8(2):31–35

Tolstoy M, Constable S, Orcutt JA, Staudigel H, Wyatt FK, Anderson G (1998) Short and long baseline tiltmeter measurements on axial seamount, Juan de Fuca Ridge. Phys Earth Planet Interiors 108:129–141

Tolstoy M, Vernon FL, Orcutt JA, Wyatt FK (2002) Breathing of the seafloor: tidal correlations of seismicity at Axial volcano. Geology 30(6):503–506

Tyler PA, Young CM (2003) Dispersal at hydrothermal vents: a summary of recent progress. Hydrobiologia 503:9–19

Varadan VK, Varadan VV (2000) Microsensors, microelectromechanical systems (MEMS), and electronics for smart structures and systems. Smart Mater Struct 9:953–972

Vasco DW, Karasaki K, Nakagome O (2002) Monitoring reservoir production using surface deformation at the Hijiori test site and the Okuaizu geothermal field, Japan. Geothermics 31(3):303–342

Willoughby EC, Letychev K, Edwards RN, Mihajlovic G (2000) Resource evaluation of marine gas hydrate deposits using seafloor compliance methods. Annals NY Acad Sci 912:146–158

Wright DJ, Haymon RM, Fornari DJ (1995) Crustal fissuring and its relationship to magmatic and hydrothermal processes on the East Pacific Rise crest (9°12′ to 54′ N). J Geophys Res 100(B4):6097–6120

Zverev SM (1997) Ocean-floor noise monitoring in the South Atlantic. Volcanol Seismol 18:703–730